Printable Bistable Structures for Programmable Frictional Skins of Soft-bodied Robots

Tung D. Ta[1] and Yoshihiro Kawahara[2]

***Abstract*— Soft robots made of flexible materials are highly adaptive, easy to fabricate, and safer to interact with. One of the ways for soft robots to interact with the surrounding environment is through their deformable bodily characteristics including internal body stiffness and external body friction. Though the flexibility of soft-bodied robots has been rigorously studied, the frictional skin of such soft-bodied robots, acting as a mechanical interface between the robot and the environment, remains unexplored. Being able to design the frictional skin will make soft-bodied robots more versatile in environmental navigation, more dexterous in manipulation tasks, and more flexible in haptic feedback. In this paper, we propose a robotic skin that can be programmed dynamically to change the mode of friction. The robotic skin is based on bistable bellow structures that can be switched between two folding states to change the contact points between the robotic skin and the ground. Our robotic skin can dynamically change its anisotropic frictional behavior to add another dimension to the designing space of soft robotics.**

I. INTRODUCTION

Soft robotics is changing the way we design, fabricate, and control robots. With the advantage of a continuous soft body, soft-bodied robots are easy to fabricate using common 2D/3D printing technologies [1], [2], [3]. The development of new printable materials makes it simpler to fine-print the body structure of the robots and add sensors/actuators during the printing phase to both complete the fabrication pipeline and close the control loop [4], [5].

However, though soft-bodied robots are usually assumed to be adaptive to the environment, in a large portion of the developed soft-bodied robots, such adaptivity is passively rooted in the intrinsic property of the deformable body. We are lacking understanding of how to cordially control the morphology of the continuum body to actively adapt and respond to the environment. Many research projects approach the challenge by tackling the stiffness of the soft body. The approaches to variable stiffness have led to many interesting results such as tendril-like soft robot [6] and jamming hand [7], [8], [9]. These research projects focused on designing the internal structure of soft-bodied robots to enable different behaviors of the body based on controlling the stiffness of the arms, fingers, or end-effectors. Nevertheless, the surficial properties of the soft body which is friction are less explored and inadequate understood. In this paper, we will address the challenge of actively programmable frictional skin for soft-bodied robots using bistable structures.

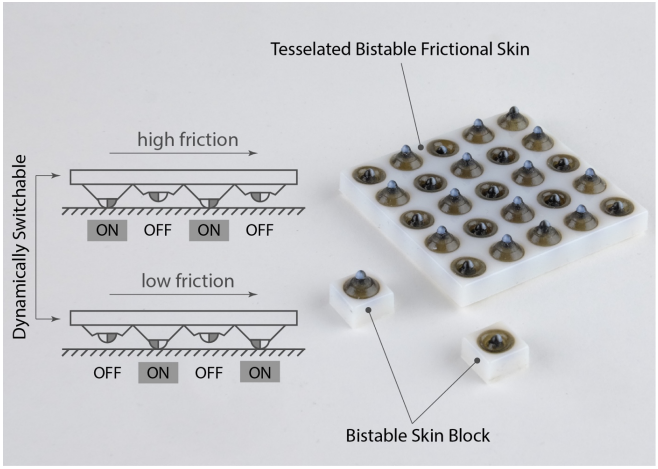

Fig. 1: A 3D-printed programmable frictional skin of soft-bodied robots that can dynamically change its frictional behaviors to adapt to the contacted surfaces. Such frictional controllability can help design more versatile soft-bodied robots in tasks such as environment exploration, manipulation, and haptic feedback.

A. Frictional Control in Soft Robots

A less explored property of a soft body is the friction between the robot and the environment. External friction decides how the robot will interact with the environment. It affects the way the robot utilizes friction and mitigates its unwanted effects to fulfill a specific task. The inching worm in [10], [11], [5], [12] all used pre-configured anisotropic frictional surfaces to make the soft robot crawl forward.

In an attempt to variable frictional surface for locomotion, the variable friction legged worm in [13] introduced the combination of high/low frictional material to achieve 1-D anisotropic frictional surface and passively coordinate with the bending motion of the body to make the inching worm move. The snake-like soft-bodied robots in [14] investigated the design of a 2-D anisotropic frictional surface and its role in forming the locomotion gaits of the snake-like soft-bodied robots. On the same line, with a different approach, the kirigami snake-like robot in [15] used a kirigami pattern to make a frictional skin that passively activates/deactivates to help the snake-like robot move forward.

*This work was supported by JSPS Grant-in-Aid for Early-Career Scientists Grant Number 20K14690, Japan

[1]Graduate School of Information Science and Technology, The University of Tokyo, 7-3-1 Hongo, Bunkyo-ku, Tokyo, Japan tung@csg.ci.i.u-tokyo.ac.jp

[2]Graduate School of Engineering, The University of Tokyo, 7-3-1 Hongo, Bunkyo-ku, Tokyo, Japan kawahara@akg.t.u-tokyo.ac.jp

Not only supporting locomotion, but the design of frictional surfaces also enables researchers to develop dexterous robot hands with the anisotropic frictional in-palm surface [16], [17]. Another research project in [18] provides a theoretical foundation to design passively friction-tunable surfaces using wrinkles.

B. Bistable Structures in Soft-bodied Robots

Bistable structures can have two stable resting states. A mechanical bistable structure uses internal elastic energy to keep it resting in one of the two stable states. To switch to another stable state, a bistable structure needs an external load larger than its intrinsic threshold load.

Bistability can be found in nature such as in the trap leaf of a Venus flying trap *Dionaea muscipula* [19], in the beak of a hummingbird [20], and in the wing of an earwig [21].

A lot of research projects took advantage of bistability to design agile motion for soft-bodied robots such as in [22], [23], [24], [25], [26], [27]. Bistability effectively helps store internal elastic energy and will rapidly release this stored energy when the structure is triggered by an adequate external load.

Bistability found its way into grasping scenarios with research in [28], [29]. These research projects took advantage of the deformability of soft bistability structures to adaptively wrap and grasp the objects.

Besides analytical studies such as in [30], [31], bistable structures are usually studied using the finite element method (FEM) as in [32], [33]. An analytical approach can provide an accurate analysis of the behavior of a bistable structure. However, it is more suitable for simple morphology with predictable non-linearity. On the other hand, the FEM approach can give a good approximation to the analysis of a bistable structure regardless of the shape and form.

In this paper, we propose the design of a robotic skin that can be programmed dynamically to change its frictional behaviors (as shown in Fig. 1). The robotic skin consists of multiple 3D-printed small blocks that are based on bistable bellow structures. We call this block a bistable skin block. When in contact with other surfaces, the bistable skin blocks can be switched between two states of touching or not touching the surfaces. The controlling of touching and not touching the surfaces define the frictional behaviors of the robotic skin. Our contributions include:

- Designing of a frictional robotic skin based on bistable bellow structure to control the frictional behaviors,
- Analysis and evaluation of the performance of bistable bellow structure and the frictional robotic skin.

II. FRICTIONAL ROBOTIC SKIN DESIGN

In this paper, we report the design of a frictional robotic skin that can change its frictional behavior dynamically. To achieve this goal, we design the skin with multiple bistable skin blocks that can be turned on/off to express different frictional coefficients.

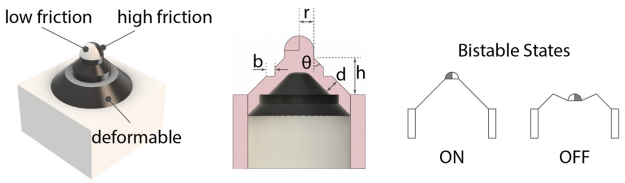

Fig. 2: The frictional robotic skin consists of multiple bistable cells/blocks that can switch their states to control the contacts between the skin and the external surface. Each cell might be turned on/off to summarily express the frictional behaviors of the robotic skin.

A. Design of a Bistable Skin Block

One of the key points of our frictional robotic skin is the ability to change its frictional behavior dynamically. In our previous research [14], we knew that it is possible to design the frictional coefficient of a robotic skin by combining different high/low frictional materials in each skin block. Based on this research, we improve the controllability of the frictional skin by introducing a bistable structure to each skin block so that the designed frictional behavior can be turned on/off dynamically.

We design a cone-shaped bellow bistable structure as shown in Fig. 2 to control the contacting state between the skin block and the external surfaces. Our frictional skin block comprises three main parts: (1) a bistable cone, (2) an anisotropic frictional tip, and (3) a base.

1) Bistable Cone: : The bistable cone is a switch in each skin block that can be turned on/off to decide whether the skin block touches the external surface or not. When the skin block touches the surface, its frictional behavior will be expressed, and ineffective otherwise. In this research, we design a bistable cone made of flexible materials such as rubber and silicone (as shown in Fig. 2). The parameters for designing the cone are listed in Table I. When turned on, the cone will be resting at its normal cone-shaped. On the other hand, when turned off, the cone will be folding at burrow b_1 and b_2 to form a conical bellow (as shown in Fig. 2). Along with the properties of the flexible material, these morphologic parameters will affect the threshold force required to fold and unfold the cone. In this paper, we will fix all parameters except the thickness d of the cone because it is the parameter that will not change the shape of the cone too much, yet have a huge influence on the threshold force and the foldability of the cone.

2) Anisotropic Frictional Tip: : The frictional anisotropy is designed by combining high/low frictional materials in a semi-sphere. In this research, for simplicity, we focus on designing a semi-sphere consisting of two quarter-spheres that are made from materials with different frictional coefficients.

3) Base: : The base acts as a platform for the cone to stick on. The base of multiple skin blocks will be joined to form a pad when multiple skin blocks are used to make a larger frictional robotic skin. This base can be the housing of wiring, tubing, and control mechanisms. However, such

TABLE I: Parametric design of a bistable skin block

Parameter	Value
Cone height h	$h = 2.5\,\text{mm}$
Cone thickness d	$d = \{0.5\,\text{mm}, 0.75\,\text{mm}, 1\,\text{mm}\}$
Tip radius r	$r = 1\,\text{mm}$
Opening angle θ	$\theta = 45°$
Burrow edge b	$b = 0.6d$
Grid size g	$g = 5 \times 5$
Cell size c	$c = 9\,\text{mm}$
Spacing s	$s = 2\,\text{mm}$
Cone material	Tango Black Plus [34]
Base material	Vero White [35]
High frictional material	Tango Black Plus [34]
Low frictional material	Vero White [35]

investigations are out-of-scope of this paper, we will only design the base as a host for the cone-shaped bellow bistable structure. Though we can use deformable material to make the base part, for the simplicity of the measurement later, we will use rigid material to print the base part.

B. Design of Assembled Skins

Our bistable robotic skins are built by tessellating the bistable skin block mentioned in II-A. The most straightforward way of tesselation is to join all the bases of multiple bistable skin blocks into a square grid with grid size g, cell size c, and spacing s as shown in Fig. 3. Though it is possible to make the base of each bistable skin block from flexible materials, for simple mechanical measuring in the experiment part, we will fabricate the base from a rigid material. Detail can be found in Table I. Each cell of the grid can get a bistable skin block with one of the four patterns of the frictional tips (as illustrated in Fig. 9).

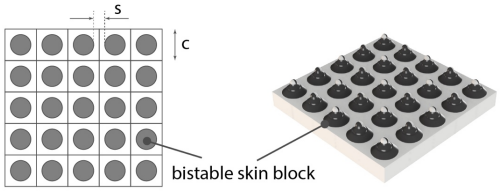

Fig. 3: We tesselate multiple bistable skin blocks into a square grid to form bistable robotic skins.

C. Fabrication of the Bistable Robotic Skin Sample

Our bistable robotic skins are made of high-frictional flexible material and low-frictional rigid material. We use a multi-material inkjet 3D printer Stratasys Objet260 Connex3 [1] to print the bistable skin block and the bistable robotic skin. We use Tango Black Plus, a rubber-like flexible material for the bistable cone and the high-frictional parts. We use Vero White, a rigid plastic material for the base and the low-frictional parts. The printed models are shown it Fig. 4

[1] https://www.stratasys.com/

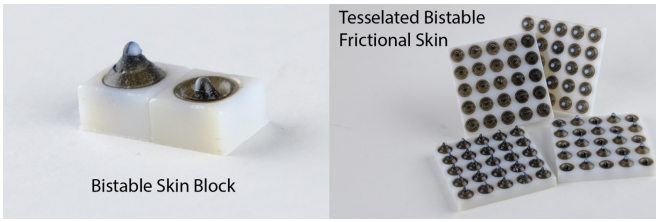

Fig. 4: Bistable skin blocks and bistable robotic skins are printed with a multi-material inkjet 3D printer. The black/dark parts are printed from high-frictional flexible Tango Black Plus. The white/light parts are printed from low-frictional rigid Vero White.

TABLE II: Mooney-Rivlin modeling of Tango Black Plus

Parameter	Value
Material constant C_{10}	$C_{10} = 0.110\,38\,\text{MPa}$ [37]
Material constant C_{01}	$C_{01} = 0.042\,28\,\text{MPa}$ [37]
Incompressibility Parameter D_1	$D_1 = 0$
Density ρ	$\rho = 1130\,\text{kg/m}^3$ [34]

III. DEFORMATION SIMULATION

This session discusses the simulation of the deformation of the bistable skin blocks. Due to the non-linearity of the deformable materials, it is generally difficult to conduct an analytical simulation of the deformation of these 3D models. In this study, we use the finite element method (FEM) to analyze the bistable skin blocks' deformation, stress, and strain. The simulation is conducted on ANSYS 2023 with Static Structural Module and hyperelastic materials.

A. Material Modeling

In this paper, we approximate the behavior of Tango Black Plus as an incompressible polymer using a Two-parameter Mooney-Rivlin model [36] with the value of parameters listed in Table II. The stress-strain curve of the Tango Black Plus is shown in Fig. 5. Ideally, as the rigid part (printed from Vero White) will not undergo any deformation, we will model it as the built-in Structural Steel in ANSYS.

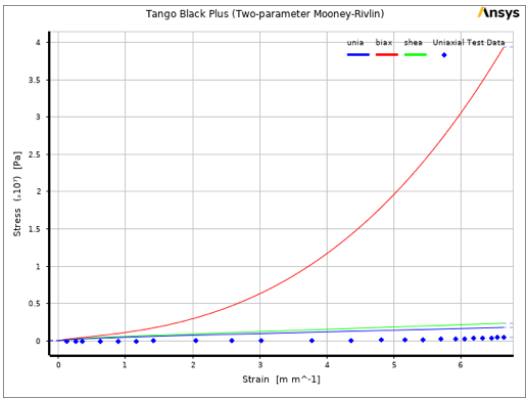

Fig. 5: Flexible material Tango Black Plus is modeled with a Two-parameter Mooney-Rivlin model. This model will be used in the FEM analysis.

B. Simulation

We simulate the deformation of the bistable skin block using ANSYS. As mentioned in II-A, we have three types of bistable skin blocks T_{050}, T_{075}, and T_{100} with different thicknesses of the cone domain $d = 0.5\,\text{mm}$, $d = 0.75\,\text{mm}$, and $d = 1\,\text{mm}$, respectively.

We keep the base fixed and set the tip of the cone to make a displacement of $\Delta l = 2\,\text{mm}$ toward the base. The simulation result is shown in Fig. 6.

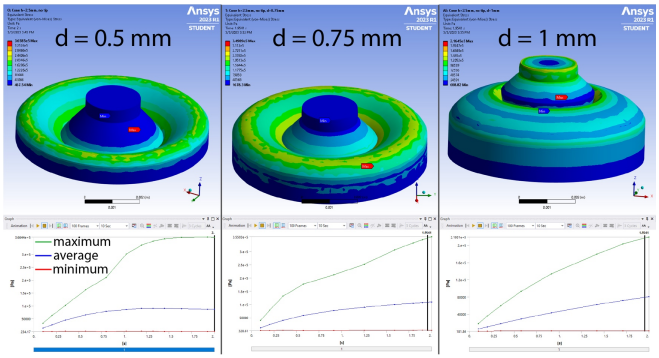

Fig. 6: Simulation of bistable deformation with three types of bistable skin block: (left) T_{050} with $d = 0.5\,\text{mm}$, (middle) T_{075} with $d = 75\,\text{mm}$, and (right) T_{100} with $d = 1\,\text{mm}$.

The prediction of the simulation points out that all three types of the bistable skin block demonstrate a slight flattening of maximum stress. This flattening is one of the telltales of a snap-through buckling. This change of stress also manifests in the visual transition of the cone into the conical bellow. However, it is not clear in the simulation whether this change of stress results in a bistable snap-through buckling, in which, the conical bellow will keep its state. In order to check this question, we will move to the physical experimental part.

IV. EXPERIMENT

This section will validate the prediction of the simulation III mentioned above. We will test the snap-through bistable buckling of the cone and the multimode friction of a designed bistable robotic skin.

A. Reaction force threshold

Same as the simulation part, this experiment section will test the snap-through bistable buckling of the cone T_{050}, T_{075}, and T_{100}. We use a tabletop force tester A&D MCT-2150 [2] to test the threshold force that needs to apply to the tip of the block, making its move, switching state, keeping the new state.

1) Experiment Setup: The bistable skin block is clamped on the bed of the force tester. There is a load cell that will push and release a bistable skin block 10 times. The configuration of the experimental setup can be seen in Fig. 7.

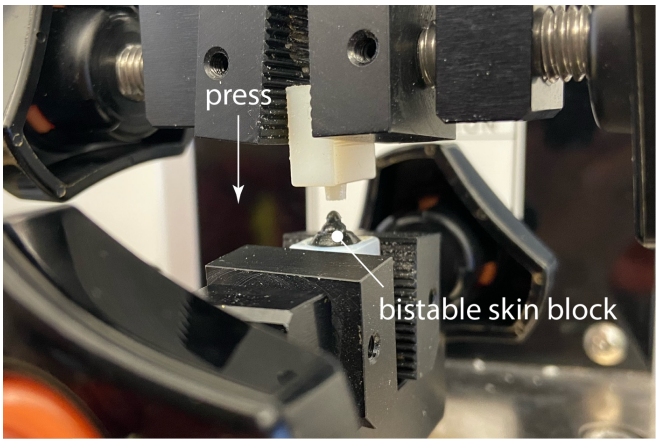

Fig. 7: We measure the reaction force of the bistable cone when pushed down by a load cell on a force tester. We experiment one by one with three types of bistable cone T_{050}, T_{075}, T_{100}

.

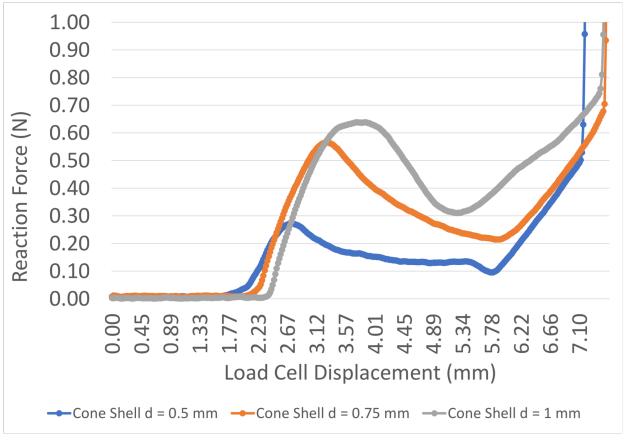

Fig. 8: The result from the push test shows that all three types of the bistable cone (T_{050}, T_{075}, T_{100}) undergo a phase of snap-through buckling. Expectedly, the thicker d of the cone shell is, the stronger the reaction force is.

2) Experiment Result: The result of the threshold force test is shown in Fig. 8. As the graph shows, all three types of the bistable cone (T_{050}, T_{075}, T_{100}) undergo a phase of snap-through buckling during the push test. The thicker d of the cone shell is, the stronger the reaction force of the cone is. However, we notice during our experiment that T_{100} will bounce back to the first resting state as soon as the load is released. T_{075} will stay at the second resting state but not stable. Just a tiny vibration will make T_{075} bounce back. T_{050} is the most stable design that can switch back and forth reliably between the two stable states. One of the plausible reasons for this difference is that the thinner cone shell allows the burrows on the cone to fold at sharper angles. Hence, the internal elastic energy of the flexible cone is not enough to bounce back the cone.

[2] https://www.aandd.jp/products/test_measuring/mct/mct.html

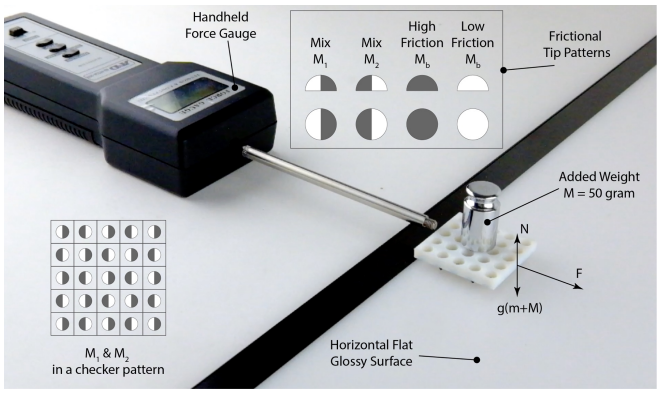

Fig. 9: We evaluate the frictional force acting on the bistable robotic skin by sliding it on a horizontal flat glossy surface. During the sliding, we measure the force needed to make it slide using a handheld force gauge. The $50\,\mathrm{g}$ added weight is for stabilizing the sliding motion by increasing the normal force.

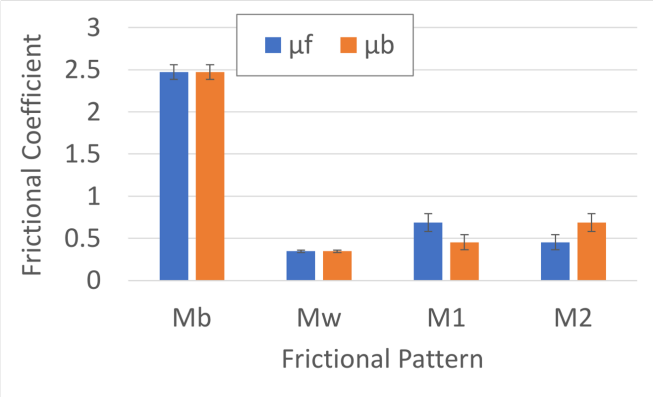

Fig. 10: The frictional coefficient between our bistable robotic skin and the horizontal flat glossy surface shows a distinction between two frictional modes. The friction of the sample when only M_1 activated is the reverse of the sample with only M_2 activated.

B. Anisotropic friction

In this section, we evaluate the frictional behavior of the bistable robotic skins while sliding on a horizontal flat glossy surface.

1) Experiment Setup: Based on the result of the bistability experiment mentioned in IV-A, only T_{050} is stable enough at both stable states. Therefore, in this anisotropic frictional experiment, we will fix the thickness of the cone shell $d = 0.5\,\mathrm{mm}$. We will change the design of the tip of the bistable skin block to achieve different frictional behaviors. As shown in Fig. 9, we will have 4 types of tips:

- M_1: left half is from a low-frictional rigid material, right half is from a high-frictional flexible material.
- M_2: left half is from a high-frictional flexible material, right half is from a low-frictional rigid material.
- M_b: the whole tip is from a high-frictional flexible material.
- M_w: the whole tip is from a low-frictional flexible material.

Our design goal is to be able to switch between different frictional behaviors without redesigning and reprinting. To achieve this goal, we tesselate the M_1 and M_2 in a checker pattern as shown in Fig. 9. In one test, the M_1 will be activated, the M_2 will be deactivated, and vice-versa. The frictional result of all M_b and all M_w is used as a baseline for comparison.

We evaluate the frictional coefficient of the bistable robotic skin with a horizontal flat glossy surface by using a handheld force gauge (A&D AD-4932A-50N[3]) to measure the external force required to make the bistable robotic skin start to move. We add a weight ($M = 50\,\mathrm{g}$) on top of the bistable robotic skin to increase the normal force, and thus, stabilize the sliding motion. The frictional coefficient of the bistable robotic skin on the horizontal flat glossy surface is calculated by the equation:

$$\mu = \frac{F}{N} = \frac{F}{g(m+M)} \tag{1}$$

where μ is the sliding frictional coefficient, F is the force required to make the bistable robotic skin move, N is the normal force the horizontal flat glossy surface acts on the bistable robotic skin, $g = 9.8\,\mathrm{m/s^2}$ is the gravitational acceleration rate, $m = 9\,\mathrm{g}$ is the mass of the bistable robotic skin, $M = 50\,\mathrm{g}$ is the mass of the added weight.

2) Experiment Result: The result of the frictional test is shown in Fig. 10. With forward direction from left to right, the sample with only M_1 activated has a higher forward frictional coefficient μ_f than the backward frictional coefficient μ_b. On the other hand, when all M_1 are deactivated and only M_2 are activated, the frictional behavior of the bistable robotic skin is reverted with $\mu_f < \mu_b$.

Taking the frictional coefficient of the all high frictional material pattern M_b and the all low frictional material pattern M_w as baselines, we can see that the frictional coefficients of the mixed pattern M_1 and M_2 are in a close approximation. It is noticeable that the frictional coefficient of an all-high-frictional material M_b is much higher than the rest. We reason that the mix of low-frictional material in other patterns makes them easier to slide. During the experiment with M_1 and M_2, we are aware that when the added weight is too high, the cone will bend backward causing the forward frictional coefficient of M_1 and backward frictional coefficient of M_2 to come close to the frictional coefficient of M_b.

V. DISCUSSION AND FUTURE WORKS

By designing a cone-shaped bistable skin block with combinations of high/low frictional materials, we can dynamically control the frictional behavior of bistable robotic skin. In this paper, though we only tesselate two frictional patterns M_1 and M_2 evenly in a square grid, we can arrange the distribution of these frictional patterns differently to

[3]https://www.aandd.jp/

dynamically achieve richer flexibility in frictional behaviors. We are not limited in the half-half pattern as M_1 and M_2 but can freely combine the high/low frictional materials to add another dimension to the designing space of the programmable frictional skins.

In the future, we are aiming at improving the performance and controllability of the programmable frictional robotic skins as follows:

- *Controllable bistable switch:* Currently, we need to manually switch the state of the bistable skin block to turn the frictional behavior on or off. It is possible to add a pneumatic mechanism to make the skin programmable in real-time.
- *Bistability optimization:* We will finetune the geometric parameters of the bistable structure to optimize the stability and flexibility of the bistable conical bellow structure.
- *Different mode of bistability:* In this paper, we focused on the linear motion bistable snap-through buckling because it is the simplest one to evaluate. We are setting our gaze on other modes of bistable buckling such as rotational buckling in a Kresling tube. Being able to control the rotational angle of the bistable skin block will enable us to design much richer frictional behavior.
- *Application in locomotion:* Being able to dynamically change frictional behavior will enable locomotion soft robots to better adapt to the surrounding environment. We are planning to integrate this programmable frictional robotic skin on stringy soft robots such as soft snake-like robots to increase the locomotion gaits and improve its locomotion flexibility.
- *Miniaturization for grasping and interaction task:* Currently, the bistable skin block is rather large so it makes the programmable frictional robotic skin rough. Even though it can function well for a set of locomotion tasks, we will shrink the size of the skin block to increase the resolution of the programmable frictional robotic skin. With a smoother robotic skin, we will use it in grasping and interaction tasks.

VI. CONCLUSIONS

In this paper, we proposed an approach to design programmable frictional robotic skins for soft-bodied robots. The programmability of the skin is based on the bistable switches of multiple conical bellow-shaped bistable skin blocks. We evaluated the bistability response of each bistable skin block and the frictional coefficient of the tesselated robotic skin. Being able to program the frictional behavior of the robotic skin opens a wide spectrum of applications such as making highly adaptive locomotion soft robots, developing dexterous grasping hands, haptic feedback, and interaction.

ACKNOWLEDGMENT

JSPS Grant-in-Aid for Early-Career Scientists Grant Number 20K14690, Japan.

REFERENCES

[1] B. Trimmer, J. A. Lewis, R. F. Shepherd, and H. Lipson, "3D printing soft materials: What is possible?" *Soft Robotics*, vol. 2, no. 1, pp. 3–6, 2015.

[2] J. Z. Gul, M. Sajid, M. M. Rehman, G. U. Siddiqui, I. Shah, K.-H. Kim, J.-W. Lee, and K. H. Choi, "3D printing for soft robotics–a review," *Sci. Technol. Adv. Mater.*, vol. 19, no. 1, pp. 243–262, 2018.

[3] M. Tyagi, G. M. Spinks, and E. W. H. Jager, "3D printing microactuators for soft microrobots," 2020.

[4] R. Niiyama, X. Sun, C. Sung, B. An, D. Rus, and S. Kim, "Pouch motors: Printable soft actuators integrated with computational design," *Soft Robotics*, vol. 2, no. 2, pp. 59–70, Jun. 2015.

[5] T. D. Ta, T. Umedachi, and Y. Kawahara, "Instant inkjet actuators and sensors for soft-bodied crawling robots," in *2019 IEEE International Conference on Robotics and Automation (IEEE ICRA'19)*. IEEE, May 2019, pp. 3658–3664.

[6] I. Must, E. Sinibaldi, and B. Mazzolai, "A variable-stiffness tendril-like soft robot based on reversible osmotic actuation," *Nat. Commun.*, vol. 10, no. 1, p. 344, Jan. 2019.

[7] E. Brown, N. Rodenberg, J. Amend, A. Mozeika, E. Steltz, M. R. Zakin, H. Lipson, and H. M. Jaeger, "Universal robotic gripper based on the jamming of granular material," *Proceedings of the National Academy of Sciences*, vol. 107, no. 44, pp. 18 809–18 814, 2010.

[8] J. Amend, N. Cheng, S. Fakhouri, and B. Culley, "Soft robotics commercialization: Jamming grippers from research to product," *Soft Robot*, vol. 3, no. 4, pp. 213–222, Dec. 2016.

[9] G. B. Crowley, X. Zeng, and H.-J. Su, "A 3D printed soft robotic gripper with a variable stiffness enabled by a novel positive pressure layer jamming technology," *IEEE Robotics and Automation Letters*, vol. 7, no. 2, pp. 5477–5482, Apr. 2022.

[10] V. Vikas, E. Cohen, R. Grassi, C. Sözer, and B. Trimmer, "Design and locomotion control of a soft robot using friction manipulation and Motor–Tendon actuation," *IEEE Trans. Rob.*, vol. 32, no. 4, pp. 949–959, Aug. 2016.

[11] T. Umedachi, T. Kano, A. Ishiguro, and B. A. Trimmer, "Gait control in a soft robot by sensing interactions with the environment using self-deformation," *R Soc Open Sci*, vol. 3, no. 12, p. 160766, Dec. 2016.

[12] N. Asawalertsak, F. Heims, A. Kovalev, S. N. Gorb, J. Jørgensen, and P. Manoonpong, "Frictional anisotropic locomotion and adaptive neural control for a soft crawling robot," *Soft Robot*, Nov. 2022.

[13] T. Umedachi, V. Vikas, and B. A. Trimmer, "Highly deformable 3-D printed soft robot generating inching and crawling locomotions with variable friction legs," in *2013 IEEE/RSJ International Conference on Intelligent Robots and Systems*. IEEE, Nov. 2013, pp. 4590–4595.

[14] T. D. Ta, T. Umedachi, and Y. Kawahara, "Design of frictional 2D-Anisotropy surface for wriggle locomotion of printable Soft-Bodied robots," in *2018 IEEE International Conference on Robotics and Automation (ICRA)*. IEEE, May 2018, pp. 6779–6785.

[15] A. Rafsanjani, Y. Zhang, B. Liu, S. M. Rubinstein, and K. Bertoldi, "Kirigami skins make a simple soft actuator crawl," *Science Robotics*, vol. 3, no. 15, p. eaar7555, Feb. 2018.

[16] A. J. Spiers, A. S. Morgan, K. Srinivasan, B. Calli, and A. M. Dollar, "Using a Variable-Friction robot hand to determine proprioceptive features for object classification during Within-Hand-Manipulation," *IEEE Trans. Haptics*, vol. 13, no. 3, pp. 600–610, Jul. 2020.

[17] T. Onodera, N. Iwamoto, and T. Umedachi, "In-hand manipulation exploiting bending and compression deformations of Caterpillar-Locomotion-Inspired fingers," in *2022 IEEE/RSJ International Conference on Intelligent Robots and Systems (IROS)*, Oct. 2022, pp. 1188–1195.

[18] H. X. Trinh, V. A. Ho, and K. Shibuya, "Theoretical foundation for design of Friction-Tunable soft finger with wrinkle's morphology," *IEEE Robotics and Automation Letters*, vol. 4, no. 4, pp. 4027–4034, Oct. 2019.

[19] A. G. Volkov, T. Adesina, V. S. Markin, and E. Jovanov, "Kinetics and mechanism of dionaea muscipula trap closing," *Plant Physiol.*, vol. 146, no. 2, pp. 694–702, Feb. 2008.

[20] M. L. Smith, G. M. Yanega, and A. Ruina, "Elastic instability model of rapid beak closure in hummingbirds," *J. Theor. Biol.*, vol. 282, no. 1, pp. 41–51, Aug. 2011.

[21] K. Saito, R. Pérez-de la Fuente, K. Arimoto, Y. A. Seong, H. Aonuma, R. Niiyama, and Z. You, "Earwig fan designing: Biomimetic and evolutionary biology applications," *Proc. Natl. Acad. Sci. U. S. A.*, vol. 117, no. 30, pp. 17 622–17 626, Jul. 2020.

[22] S. Nishikawa, Y. Arai, R. Niiyama, and Y. Kuniyoshi, "Coordinated use of Structure-Integrated bistable actuation modules for agile locomotion," *IEEE Robotics and Automation Letters*, vol. 3, no. 2, pp. 1018–1024, Apr. 2018.

[23] Y. Sugiyama and S. Hirai, "Crawling and jumping of deformable soft robot," in *2004 IEEE/RSJ International Conference on Intelligent Robots and Systems (IROS) (IEEE Cat. No.04CH37566)*. IEEE, Sep. 2004, pp. 3276–3281.

[24] A. Yamada, M. Watari, H. Mochiyama, and H. Fujimoto, "A jumping robot based on the closed elastica," in *2007 International Symposium on Micro-NanoMechatronics and Human Science*, Nov. 2007, pp. 604–609.

[25] J.-S. Koh, S.-P. Jung, R. J. Wood, and K.-J. Cho, "A jumping robotic insect based on a torque reversal catapult mechanism," in *2013 IEEE/RSJ International Conference on Intelligent Robots and Systems*, Nov. 2013, pp. 3796–3801.

[26] T. D. Ta, T. Umedachi, and Y. Kawahara, "A multigait stringy robot with bi-stable soft-bodied structures in multiple viscous environments," in *2020 IEEE International Conference on Intelligent Robots and Systems (IEEE IROS'20)*. IEEE, Oct. 2020.

[27] T. D. Ta, Z. Chang, K. Narumi, T. Umedachi, and Y. Kawahara, "Printable origami bistable structures for foldable jumpers," in *2022 International Conference on Robotics and Automation (ICRA)*. IEEE, May 2022.

[28] Z. Zhang, X. Ni, H. Wu, M. Sun, G. Bao, H. Wu, and S. Jiang, "Pneumatically actuated soft gripper with bistable structures," *Soft Robot.*, no. soro.2019.0195, Jan. 2021.

[29] H. Yasuda, K. Johnson, V. Arroyos, K. Yamaguchi, J. R. Raney, and J. Yang, "Leaf-Like origami with bistability for Self-Adaptive grasping motions," *Soft Robot*, Apr. 2022.

[30] S. D. Guest and S. Pellegrino, "Analytical models for bistable cylindrical shells," *Proceedings of the Royal Society A: Mathematical, Physical and Engineering Sciences*, vol. 462, no. 2067, pp. 839–854, Jan. 2006.

[31] P. M. Sobota and K. A. Seffen, "Bistable polar-orthotropic shallow shells," *R Soc Open Sci*, vol. 6, no. 8, p. 190888, Aug. 2019.

[32] T. Smit, "Finite element modeling of non-rigid origami: Parametric study on bistable origami using the finite element method," Ph.D. dissertation, Delft University of Technology, Jul. 2017.

[33] B. Wang, C. Ge, and K. S. Fancey, "Snap-through behaviour of a bistable structure based on viscoelastically generated prestress," *Composites Part B*, vol. 114, pp. 23–33, Apr. 2017.

[34] Stratasys Inc., "Tango: A soft flexible 3d printing material," Feb. 2023. [Online]. Available: https://www.stratasys.com/en/materials/materials-catalog/polyjet-materials/tango/

[35] ——, "Vero: A realistic multi-color 3d printing material," Feb. 2023. [Online]. Available: https://www.stratasys.com/en/materials/materials-catalog/polyjet-materials/vero/

[36] J. Bergstrom, *Mechanics of Solid Polymers Theory and Computational Modeling*. Elsevier, 2015.

[37] E. S. Lopez, "A study on the material characterization and finite element analysis of digital materials and their applications," Ph.D. dissertation, Purdue University, Dec. 2017.